Monthly Notices of the ROYAL ASTRONOMICAL SOCIETY

MNRAS **524,** L1–L4 (2023) https://doi.org/10.1093/mnrasl/slad066
Advance Access publication 2023 June 6

Characterizing asteroid (152830) Dinkinesh in preparation for the encounter with the NASA Lucy mission: a photometric study

Stefano Mottola [1]★ Tilmann Denk,[1] Simone Marchi,[2] Richard P. Binzel,[3] Keith S. Noll,[4] John R. Spencer[2] and Harold F. Levison[2]

[1]*Institute of Planetary Research, German Aerospace Center (DLR), Rutherfordstr. 2, D-12489 Berlin, Germany*
[2]*Southwest Research Institute, 1050 Walnut Street, Boulder, CO 80302, USA*
[3]*Department of Earth, Atmospheric, and Planetary Sciences, Massachusetts Institute of Technology, Cambridge, MA 02139, USA*
[4]*Goddard Space Flight Center, 8800 Greenbelt Road, Greenbelt, MD 20771, USA*

Accepted 2023 June 1. Received 2023 June 1; in original form 2023 May 16

ABSTRACT

Main Belt asteroid (152830) Dinkinesh will be the first fly-by target of the Lucy mission on 2023 November 1, during its cruise to the Trojan clouds. We report our photometric time series observations of this target performed on 14 nights over nearly three months during the 2022-23 apparition with the 1.23-m telescope at Calar Alto, Spain, aimed at determining its rotation and photometric properties. We find that Dinkinesh is a slow rotator ($P_{\rm syn} = 52.67 \pm 0.04$ h) with a moderately large light-curve amplitude ($A = 0.39 \pm 0.02$), which implies an axial ratio $a/b \gtrsim 1.43$. Its photometric parameters in the HG-system are $H_{\rm R} = 17.17 \pm 0.04$ and $G_{\rm R} = 0.378 \pm 0.035$ with a colour index V–R $= 0.455 \pm 0.025$. A fit to the IAU H, G_1, G_2 system results in $H_{\rm R-(H,G_1,G_2)} = 17.17 \pm 0.14$; $G_1 = 0.37 \pm 0.17$ and $G_2 = 0.43 \pm 0.04$. Assuming that Dinkinesh's albedo lies within $\pm 2\sigma$ of the average value for small S-class asteroids, its spherical surface-equivalent diameter is between 0.66 and 1.36 km.

Key words: techniques: photometric – minor planets, asteroids: individual: (152830) Dinkinesh.

1 INTRODUCTION

Asteroid (152830) Dinkinesh (formerly known with its provisional designation 1999 VD57) has recently been selected to be the first fly-by target of the NASA Lucy mission, currently on the course of its journey to the Jupiter trojan clouds. A search for opportunities of fly-bys with main belt asteroids (MBAs) by the Lucy Science Team revealed one exceptionally close encounter with the Lucy spacecraft coming within 64 000 km of Dinkinesh on 2023 November 1. With a planned small delta-v maneuver, the spacecraft trajectory will be adjusted to approach the asteroid to about 425 km. The design goal was to obtain an encounter with a slew rate and a viewing geometry similar to the one for the trojan targets, to allow the spacecraft to rehearse its autonomous terminal tracking capability and to enable the onboard payload suite to acquire useful science data.

Very little was known about Dinkinesh at the time the close-approach opportunity was identified, with the available information limited to its orbital parameters and an approximate absolute ($H_{\rm V}$) magnitude of 17.4 (*MPO 694373*[1]). Quite conveniently, however, this comparatively faint object reached opposition geometry in December 2022, prompting reconnaissance observations by a few teams.

Two groups of observers have reported visible spectroscopic observations of Dinkinesh. Bolin et al. (2023) obtained a spectrum from the Keck telescope's Low Resolution Imaging Spectrometer on 2022 November 23 and a second spectrum from the Gemini-South Multi-Object Spectrograph on 2022 December 27. de León et al. (2023) obtained a spectrum with the OSIRIS camera-spectrograph at the 10.4-m Gran Telescopio Canarias on 2022 December 2. Both teams compared their spectra to a template of spectral types from DeMeo et al. (2009) and found the best match with Sq- or S- spectral types. The spectral type can be used to infer the albedo of the object.

Also our team took advantage of the 2022–2023 apparition, and performed photometric time series observations of Dinkinesh. Our goal was to determine its – yet unknown – rotation and photometric properties. We combine the improved absolute magnitude we measure with the albedo inferred from spectral measurements to derive an estimated diameter range below. Knowledge of the photometric and rotation properties of Dinkinesh is critical for the planning of the encounter target acquisition exposure times and also for the interpretation of science data returned by the spacecraft.

2 OBSERVATIONS

The asteroid crossed the Galactic plane during the 2022–2023 apparition, which, due to the corresponding crowded fields and the object's comparably faint apparent magnitude (between V=19 and 21), made Dinkinesh a difficult target. For this campaign, a total of 20 nights in the period November 2022–February 2023 were allocated from the DLR guaranteed time contingent at the 1.23-m telescope in Calar Alto, Spain (observatory code 493), out of which, 14 were of useful quality. The illumination geometry covered quite an ample range in solar phase angle (2.9–23.5 deg), approaching the minimum phase angle of 2.3° achievable during this apparition. In

★ E-mail: stefano.mottola@dlr.de
[1]https://minorplanetcenter.net/iau/ECS/MPCArchive/2022/MPO_20220520.pdf

order to optimize telescope-time usage, exposures were scheduled for epochs at which the object was not proximate to stars brighter than V $\simeq$ 21.5, based on the object's ephemeris and on star charts. The telescope was tracked at half the apparent motion vector of the target, in order to obtain similar point spread functions (PSFs) for the target and the field stars, making a photometric aperture correction unnecessary. In this way, exposures of 300 s resulted in trails with an elongation smaller than 1 arcsec. Instead of pointing the telescope each night at the target's position, we rather aimed it to the same stellar field on consecutive nights, until the target moved to an adjacent field. With the telescope field of view of 22 arcmin, we could use exactly the same set of comparison stars on a few consecutive nights (typically between three and five), depending on Dinkinesh's apparent motion. With this technique the night-to-night zero-point consistency is improved, which proves valuable especially when observing targets with long periods of rotation. Observations were mainly carried out in the Cousins R_C filter, and, during one night, by alternating the R_C with the Johnson V filter (see Table 1).

3 DATA REDUCTION AND ANALYSIS

The raw images were pre-processed with bias frames and twilight sky flat-fields acquired daily, following standard practices. Aperture photometry was performed with the AstPhot data reduction package (Mottola et al. 1995). Faint stars still present on the path of Dinkinesh were measured on several frames on multiple nights, in order to obtain a high-SNR magnitude, and then their flux subtracted from the target's during close appulses. We find that this procedure produces more accurate results than subtracting the field stars in image space, especially during nights with variable seeing. Reduction to the standard Johnson system was performed by using the Gaia DR2 catalogue (Gaia Collaboration 2018), with the colour transformations reported in Evans et al. (2018). Typically, 26 in-field high-SNR Gaia stars were used as comparison. Mutual flux ratios of the stars were checked to identify variability and eliminate outliers. Typical internal RMS accuracy of the photometric zero-points was of the order of 12 mmag, while typical SNR for the target ranged from 25 to 30 in the R_C band and from 15 to 20 in the V band.

We also routinely measured astrometric positions of the target that were reported to the Minor Planet Center and helped refine its orbit in view of the Lucy encounter.

One of the important goals of repeated photometric observations was to constrain the rotation state of the asteroid. de León et al. (2023) set an upper limit to variability of about 0.1 mag over a 6-hr photometric times series they obtained on 17 November 2022.

During the observations reported here it became apparent that Dinkinesh showed small intra-night intensity variations and a substantial night-to-night light-curve variation. A rotation period analysis performed with the Lomb method (Press et al. 1992) revealed a strong signal peak at a frequency $f_1 \simeq 0.91\ \mathrm{d}^{-1}$. The fine period search was performed with the Fourier-analysis method described in Harris et al. (1989), modified to simultaneously solve for synodic period, phase coefficient of the HG-system and V–R colour index. With this method, the best set of parameters is sought that minimizes the residuals, with the light-curve composite expressed as a low-order Fourier polynomial as a function of the rotational phase. The light-curve is reduced to a reference phase angle and to unit distance from the observer and from the Sun, with the optimization being performed in magnitude space. The resulting zeroth coefficient of the best-fitting Fourier polynomial corresponds to the average light-curve magnitude at the reference solar phase, which can be used to compute the absolute magnitude H by using the best-fitting G-parameter. All observations were expressed in their measured Johnson magnitudes, and no arbitrary magnitude shift was applied during the period determination procedure.

4 RESULTS AND DISCUSSION

By assuming a light curve with two pairs of extrema, we find an unambiguous synodic rotation period $P_{\mathrm{syn}} = 52.67 \pm 0.04$ h, corresponding to a frequency of $f_1/2$. The light curve maximum amplitude has been determined to be $A = 0.39 \pm 0.02$. Fig. 1 shows a composite of the Dinkinesh light curve.

The best-fitting HG-system parameters for the R band are $H_R = 17.17 \pm 0.04$, and $G_R = 0.378 \pm 0.035$, measured for the light-curve mean brightness. The V–R colour index is 0.455 ± 0.025. Although the G_V value has not been directly measured, using G_R as a proxy for G_V (thereby neglecting phase-reddening effects) results in $H_V = 17.62 \pm 0.04$. The phase curve is shown in Fig. 2, with the solid line corresponding to the best-fit HG-function. The symbols have been computed from the light-curve data by subtracting the modelled rotational component and by binning the resulting values within each observing night. In the figure, synthetic phase curves of a few reference S-type asteroids are also shown for context.

We also expressed the phase curve in the more recently IAU-adopted H, G_1, G_2 system (Muinonen et al. 2010). For this purpose we used the tool described in Penttilä et al. (2016) and performed a linear unconstrained fit. The results are summarized in Table 2.

A statistical correlation has been reported between an object's location in the G_1, G_2 space and its taxonomic group (Penttilä et al. 2016; Shevchenko et al. 2016). By exploiting this correlation, the tool by Penttilä et al. (2016) performs a tentative unsupervised taxonomic association to one of five possible groups: C, E, D, P, and S/M. The most statistically significant match to the phase curve of Dinkinesh is given by this latter group, though the membership to an S or M type cannot be resolved based on photometric data alone. This result, however, independently supports the findings by de León et al. (2023) and Bolin et al. (2023) that Dinkinesh belongs to the S spectral complex.

With our newly determined absolute magnitude it is possible for us to determine an effective diameter for Dinkinesh. Given that no direct radiometric determination of the albedo is yet available for this object, we also – as de León et al. (2023) and Bolin et al. (2023) – consider an average value for the S class, mostly derived from WISE measurements (Mainzer et al. 2011; Masiero et al. 2011). However, Pravec et al. (2012) have shown that currently all major data bases for H values suffer from a rather severe bias that tends to overestimate the absolute brightness of objects fainter than $H_V \approx 14$. This bias, the cause of which is not fully understood, has propagated into the determinations of albedos, thereby producing overestimated albedos for the smaller objects. Pravec et al. (2012) state that the observed brightening of small S-type asteroids in the WISE sample is almost entirely due to this effect. We have used the revised albedo values in the sample by Pravec et al. (2012) and Binzel et al. (2004) – augmented by including more recent taxonomic classifications by Vereš et al. (2015), Binzel et al. (2019), and Hromakina et al. (2021), and updated to include results from radar imaging and space missions – to compute the average albedo of small (<25 km) S-complex asteroids (see Fig. 3). The result is a mean $p_V = 0.217 \pm 0.006$ with a standard deviation of the distribution of 0.062 on a cohort of 118 objects. By adopting these values, our H-value constrains Dinkinesh's diameter to be within the $\pm 2\sigma$ range of 0.66–1.36 km. We recall that this diameter estimation refers to the surface-equivalent diameter and not to the maximum extent of the body.

Table 1. Observational circumstances for (152830) Dinkinesh.

Date (UTC)	λ (° J2000)	β	α (°)	r (au)	Δ (au)	λ (PAB) (° J2000)	β	Band
2022 Nov 24.1	104.6	+ 3.3	20.4	1.9462	1.1057	94.5	+ 2.6	R_C
2022 Nov 26.1	104.5	+ 3.4	19.5	1.9460	1.0911	94.8	+ 2.7	R_C
2022 Nov 28.0	104.4	+ 3.4	18.7	1.9459	1.0780	95.1	+ 2.7	R_C
2022 Nov 29.1	104.4	+ 3.4	18.2	1.9458	1.0712	95.3	+ 2.7	R_C
2022 Nov 30.1	104.3	+ 3.5	17.7	1.9458	1.0642	95.4	+ 2.7	R_C
2022 Dec 16.9	101.5	+ 3.9	8.7	1.9465	0.9847	97.3	+ 3.0	R_C
2022 Dec 17.9	101.3	+ 4.0	8.1	1.9466	0.9819	97.4	+ 3.0	R_C
2022 Dec 21.2	100.5	+ 4.0	6.1	1.9471	0.9742	97.6	+ 3.0	R_C
2022 Dec 23.0	100.0	+ 4.0	5.0	1.9474	0.9710	97.7	+ 3.0	R_C
2022 Dec 25.0	99.5	+ 4.1	3.9	1.9477	0.9684	97.8	+ 3.0	R_C
2022 Dec 25.9	99.2	+ 4.1	3.4	1.9479	0.9676	97.9	+ 3.1	R_C
2022 Dec 27.0	99.0	+ 4.1	2.9	1.9481	0.9670	97.9	+ 3.1	R_C
2023 Jan 23.1	92.8	+ 3.9	14.5	1.9566	1.0408	100.0	+ 3.0	V, R_C
2023 Feb 13.9	91.9	+ 3.4	23.5	1.9679	1.2059	103.7	+ 2.8	R_C

Note. λ and β are the topocentric ecliptic longitude and latitude of the target, respectively. α is the solar phase angle, r is the heliocentric distance, and Δ is the topocentric range of the target. λ and β (PAB) are the topocentric ecliptic longitude and latitude of the phase angle bisector, as defined in Harris et al. (1984).

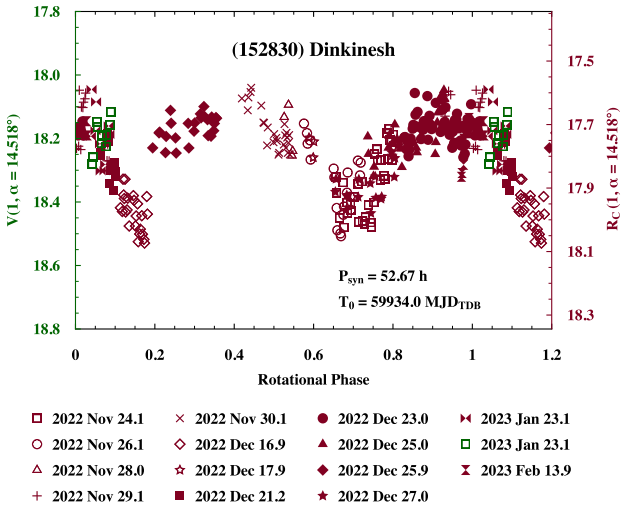

Figure 1. Composite light curve of Dinkinesh during the 2022–2023 apparition. The data points beyond rotational phase 1.0 are repeated for clarity. The reference epoch T_0 is one-leg light-time corrected and expressed in the TDB uniform frame. The magnitudes are reduced to the distance of 1 au from the Sun and from the observer and to the reference phase angle $\alpha = 14.518°$ (chosen as the average phase angle of all observations) using the obtained best-fitting G-value.

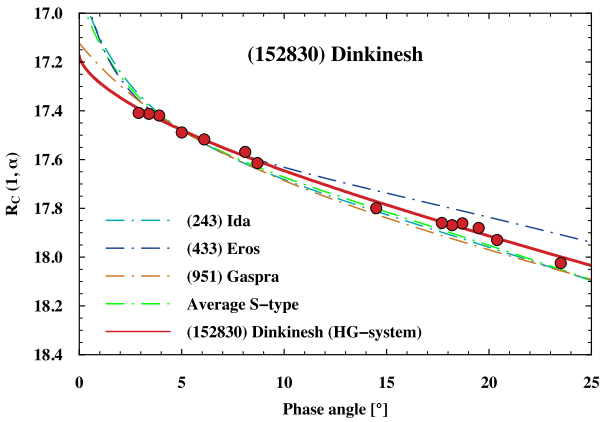

Figure 2. Phase curve of Dinkinesh in the R band. The solid line corresponds to the HG-function with the best-fitting parameters $H_R = 17.17$ and $G_R = 0.379$. See text for details. The dashed lines represent synthetic phase curves of a few reference S-type asteroids, obtained by integrating the Hapke (1993) photometric model over a sphere, with the parameters listed in Li, A'Hearn & McFadden (2004). For the purpose of comparison, the dashed curves are normalized to the magnitude value of Dinkinesh at the phase angle of 5°.

The observed random-epoch amplitude of Dinkinesh implies a lower bound for the *a*/*b* semi-axes ratio of ≈1.43, which makes it a rather elongated body. This is in contrast to similarly-sized objects as Ryugu and Bennu that have a spinning-top shape (Barnouin et al. 2019; Watanabe et al. 2019).

With its rotation period in excess of 52 h Dinkinesh qualifies as a slow rotator. This, in addition to the small size of the object, results in very long relaxation times against a possible excited rotation state. Pravec et al. (2014), who updated the estimates by Harris (1994), reckoned a relaxation time of the order of a few billion years for a body with the size and the spin rate of Dinkinesh. As a consequence, should an excited rotation have been induced in the past – either as the result of the formation process or as a post-formation collisional

Table 2. Results.

Synodic Period (h)	52.67 ± 0.04
Amplitude (mag)	0.39 ± 0.02
a/*b*	$\gtrsim 1.43$
H_V	17.62 ± 0.04
H_R	17.17 ± 0.04
G_R	0.378 ± 0.035
V − R	0.455 ± 0.025
$H_{R-(H,G_1,G_2)}$	17.17 ± 0.14
G_1	0.37 ± 0.17
G_2	0.43 ± 0.04

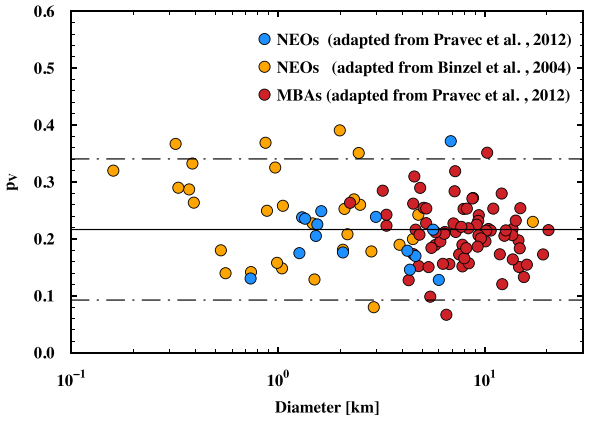

Figure 3. Plot of the geometric albedo vs. diameter for near-Earth objects (NEOs) and MBAs < 25 km belonging to the S complex. The lines define the average of the population and the $\pm 2\sigma$ region around the mean albedo.

event – its signature could still be visible now as a precession. The light-curve data at hand, however, do not have yet the coverage and accuracy necessary to test this possibility.

Until a decade ago, slow rotators were poorly represented in the statistics of asteroidal spin. However, more recently, the advent of systematic all-sky photometric surveys (both ground- and space-based) has facilitated the use of data-harvesting approaches, which has made the search for rotation periods, especially long ones, much more efficient. Examples of these studies are represented by Waszczak et al. (2015), Pál et al. (2020), and Erasmus et al. (2021). As a result, the Asteroid Lightcurve Photometry Database (Warner, Harris & Pravec 2009) contains – as of April 2023 – a total of 11 425 objects in the size range 0.3–3 km for which the rotation period is known with a reliability code U better than or equal to 2–. Of those asteroids, 1502, or about 13 per cent of the sample rotate more slowly than Dinkinesh. Considering that this fraction – due to selection bias – is probably still an underestimation, slowly rotating objects are a significant component of the small asteroid population.

It is generally accepted that the underlying mechanisms controlling the spin distribution of asteroids is the angular momentum transfer due to collisional interaction, which tends to 'thermalize' the spins towards a Maxwellian distribution (Harris & Burns 1979; Binzel 1984; Salo 1987). To this phenomenon is superimposed the thermal YORP effect (Rubincam 2000), which can contribute both to spin-up or spin-down the bodies, depending on their particular shape, and that is particularly effective for smaller objects. Another effect that can contribute to spin-down an asteroid is the separation of the components of a binary system. Which one is the actual cause for the current spin state of Dinkinesh is an open question. The close fly-by of Lucy may reveal the record of the events that shaped this object and imparted its present rotation state.

ACKNOWLEDGEMENTS

Based on observations collected at the Centro Astronómico Hispano en Andalucía (CAHA) at Calar Alto, operated jointly by Junta de Andalucía and Consejo Superior de Investigaciones Científicas (IAA-CSIC). Research at the DLR was funded by the DLR Programmatik Raumfahrtforschung und -technologie through the grant 2474029 Lucy.

DATA AVAILABILITY

The data underlying this article will be shared on reasonable request to the corresponding author.

REFERENCES

Barnouin O. S. et al., 2019, Nat. Geosci., 12, 247
Binzel R. P., 1984, Icarus, 57, 294
Binzel R. P., Rivkin A. S., Stuart J. S., Harris A. W., Bus S. J., Burbine T. H., 2004, Icarus, 170, 259
Binzel R. et al., 2019, Icarus, 324, 41
Bolin B. T., Noll K. S., Caiazzo I., Fremling C., Binzel R. P., 2023, Icarus, 400, 115562
de León J., Licandro J., Pinilla-Alonso N., Moskovitz N., Kareta T., Popescu M., 2023, A&A, 672, A174
DeMeo F. E., Binzel R. P., Slivan S. M., Bus S. J., 2009, Icarus, 202, 160
Erasmus N. et al., 2021, MNRAS, 506, 3872
Evans D. W. et al., 2018, A&A, 616, A4
Gaia Collaboration, 2018, A&A, 616, A13
Hapke B., 1993, Theory of reflectance and emittance spectroscopy. Cambridge Univ. Press, Cambridge
Harris A. W., 1994, Icarus, 107, 209
Harris A. W., Burns J. A., 1979, Icarus, 40, 115
Harris A. W., Young J. W., Scaltriti F., Zappala V., 1984, Icarus, 57, 251
Harris A. W. et al., 1989, Icarus, 77, 171
Hromakina T. et al., 2021, A&A, 656, A89
Li J., A'Hearn M. F., McFadden L. A., 2004, Icarus, 172, 415
Mainzer A. et al., 2011, ApJ, 743, 156
Masiero J. R. et al., 2011, ApJ, 741, 68
Mottola S., De Angelis G., Di Martino M., Erikson A., Hahn G., Neukum G., 1995, Icarus, 117, 62
Muinonen K., Belskaya I. N., Cellino A., Delbò M., Levasseur-Regourd A.-C., Penttilä A., Tedesco E. F., 2010, Icarus, 209, 542
Pál A. et al., 2020, ApJS, 247, 26
Penttilä A., Shevchenko V. G., Wilkman O., Muinonen K., 2016, Planet. Space Sci., 123, 117
Pravec P., Harris A. W., Kušnirák P., Galád A., Hornoch K., 2012, Icarus, 221, 365
Pravec P. et al., 2014, Icarus, 233, 48
Press W. H., Teukolsky S. A., Vetterling W. T., Flannery B. P., 1992, Numerical Recipes in C, 2nd edn., The Art of Scientific Computing. Cambridge Univ. Press, Cambridge
Rubincam D. P., 2000, Icarus, 148, 2
Salo H., 1987, Icarus, 70, 37
Shevchenko V. G. et al., 2016, Planet. Space Sci., 123, 101
Vereš P. et al., 2015, Icarus, 261, 34
Warner B. D., Harris A. W., Pravec P., 2009, Icarus, 202, 134
Waszczak A. et al., 2015, AJ, 150, 75
Watanabe S. et al., 2019, Science, 364, 268

This paper has been typeset from a TEX/LATEX file prepared by the author.